The American Journal of Pathology, Vol. 192, No. 12, December 2022

ELSEVIER

The American Journal of
PATHOLOGY
ajp.amjpathol.org

CELL INJURY, REPAIR, AGING, AND APOPTOSIS

Smurf2 Regulates Inflammation and Collagen Processing in Cutaneous Wound Healing through Transforming Growth Factor-β/Smad3 Signaling

Christina H. Stuelten,* Nicolas Melis,* Bhagawat Subramanian,* Yi Tang,* Megan Kimicata,† John P. Fisher,‡ Roberto Weigert,* and Ying E. Zhang*

From the Laboratory of Cellular and Molecular Biology, Center for Cancer Research, National Cancer Institute, NIH, Bethesda; and the Department of Materials Science and Engineering† and the Fischell Department of Bioengineering,‡ University of Maryland, College Park, Maryland*

Accepted for publication August 23, 2022.

Address correspondence to Ying E. Zhang, Ph.D., Laboratory of Cellular and Molecular Biology, Center for Cancer Research, National Cancer Institute, NIH, Bldg. 37, Room 2056B, Bethesda, MD 20892-4256.
E-mail: zhangyin@mail.nih.gov.

Wound healing is a highly conserved process that restores the integrity and functionality of injured tissues. Transforming growth factor (TGF)-β is a master regulator of wound healing, whose signaling is attenuated by the E3 ubiquitin ligase Smurf2. Herein, the roles of Smurf2 in cutaneous wound healing were examined using a murine incisional cutaneous model. Loss of *Smurf2* increased early inflammation in the wounds and led to narrower wounds with greater breaking strength. Loss of *Smurf2* also led to more linearized collagen bundles in normal and wounded skin. Gene expression analyses by real-time quantitative PCR indicated that *Smurf2*-deficient fibroblasts had increased levels of TGF-β/Smad3 signaling and changes in expression profile of genes related to matrix turnover. The effect of *Smurf2* loss on wound healing and collagen bundling was attenuated by the heterozygous loss of *Smad3*. Together, these results show that Smurf2 affects inflammation and collagen processing in cutaneous wounds by down-regulating TGF-β/Smad3 signaling. *(Am J Pathol 2022, 192: 1699–1711; https://doi.org/10.1016/j.ajpath.2022.08.002)*

Wound healing is a complex and dynamic process of replacing injured tissues and restoring the structural and functional integrity of the skin. As such, dysregulated wound healing often leads to unsightly scars and impairs tissue functions. Wound healing is characterized by a tightly regulated regenerative fibrotic process that occurs in four phases: hemostasis, inflammation, proliferation or growth of new tissue, and maturation or remodeling.[1] It is regulated by multiple signaling pathways, including those of transforming growth factor (TGF)-β and its related factors.[2] Clinically, increased TGF-β signaling is found in hypertrophic scars and in keloids.[3] During wound healing, TGF-β acts on a broad spectrum of cell types. These include keratinocytes, which are responsible for reconstruction of the cutaneous barrier; fibroblasts, which are responsible for matrix production; and innate immune cells, largely neutrophils and macrophages, which are actively recruited to the wound at an early stage and secrete multiple cell-regulatory cytokines, including TGF-β.[4]

TGF-β signals through a complex of type I and type II membrane-associated receptors.[5,6] The core conduit of downstream TGF-β signaling consists of three classes of signal transducers: the receptor-specific R-Smads, Smad2 and Smad3; the common Co-Smad, Smad4; and the inhibitory I-Smad, Smad7. Once activated by ligand engagement, TGF-β type I receptor phosphorylates Smad2 or Smad3 at its carboxyl terminus and sets forth its binding to Smad4 and transition into the nucleus, where they control target gene expression. As a key transducer of TGF-β signaling, the function of Smad3 is intimately linked to wound healing. Loss of Smad3 increases re-epithelialization of wounds and reduces immune infiltration and formation of granulation tissue in a murine model of wound healing.[7]

The E3 ubiquitin ligase Smurf2 is a negative regulator of TGF-β signaling.[8–10] Smurf2 can interact with R-Smads

Supported by the Intramural Research Program of the NIH, National Cancer Institute, Center for Cancer Research (R.W. and Y.E.Z.).
Disclosures: None declared.

https://doi.org/10.1016/j.ajpath.2022.08.002

that contain a PPxY motif, such as Smad2 and Smad3 in the TGF-β pathway.[8,11] Initial reports suggested that these R-Smads and Smurf2 interactions promote poly-ubiquitination and degradation of R-Smads. Later studies revealed that Smurf2 induces multiple mono-ubiquitination of Smad3 and inhibits the activity of Smad3 without causing its degradation.[12] Smurf2 can also interact with Smad7 and use it as an adaptor to promote turnover of ligand-activated TGF-β type I receptors, thereby turning off the receptor signaling.[13]

Despite the important roles of Smurf2 in regulating TGF-β signaling, its physiological function during wound healing has not been studied. Because Smurf2 exerts a crucial regulation of several components of the TGF-β pathway, it may offer a powerful intervening point to fine-tune the wound healing process. To this end, this study sought to understand the precise function of Smurf2 in wound healing by taking advantage of *Smurf2* knockout (*SF2KO*) mice.[12,14] A mouse model of incisional cutaneous wound healing, was used to show herein that loss of *Smurf2* narrows wounds and increases wound breaking strength, both of which are indicative of an accelerated wound repairing process. Histologically, *Smurf2* knockout led to linearized collagen bundles in skin and wounds. The effect of *Smurf2* loss on wound width and collagen bundling was attenuated by heterozygous loss of *Smad3*. Furthermore, fibroblasts isolated from *SF2KO* mice had altered expression of genes associated with matrix turnover and increased collagen gel contractility and collagenolytic activity than their wild-type (WT) counterparts. In summary, these results demonstrated that *Smurf2* plays an important role in balancing collagen production, matrix contraction, and degradation.

Materials and Methods

Animals

Smurf2 knockout (*Smurf2*$^{-/-}$; *SF2KO*) and *WT* animals on a mixed 129/SvJ × NIH Black Swiss and pure C57BL/6N background and *Smad3* knockout (*Smad3*$^{-/-}$) animals (C57BL/6N background) were previously described.[12,14,15] Animals were on a mixed 129/SvJ × NIH Black Swiss background except when mentioned otherwise in the figure legend. All mice were maintained and handled according to protocols approved by the Animal Care and Use Committee of the National Cancer Institute, NIH.

Cutaneous Wounding

Animals were anesthetized with buprenorphine LAB SR (0.8 mg/kg, subcutaneously; ZooPharm, Laramie, WY) and isoflurane (Baxter, Deerfield, IL) by inhalation to effect. The back of animals was shaved and disinfected with 2% chlorhexidine (Santa Cruz Animal Health, Dallas, TX) before wounding. Full-thickness incisional wounds (10 mm) parallel to the spine were made using a scalpel. The wound edges were adapted at the corners of the wound with Prolene 5-0 single-stitch sutures (Ethicon, Cornelia, GA).

Wound Breaking Strength

Wound breaking strength was analyzed with an Instron 5565 Universal Testing Machine (Instron, Norwood, MA) 14 days after wounding on 5-mm−wide skin strips that were cut perpendicular to the wound.

Histology

Tissues were fixed in 4% neutral-buffered paraformaldehyde, then dehydrated and embedded in paraffin using routine procedures. Specifically, to obtain oriented sections of wounds, skin containing the wound was spread face up on Whatman paper before formaldehyde fixation. The fixed tissue was then trimmed to obtain wound-containing strips perpendicular to the wound and embedded on edge in paraffin to obtain cross-sections of the wound. CD45 staining (anti-CD45; number 550539; BD Biosciences, San Jose, CA) was performed by Frederick National Laboratory for Cancer Research (Frederick, MD) using routine procedures. Degraded collagen was visualized by incubation of deparaffinized sections with 10 μmol/L Cy3-conjugated collagen hybridization peptide (R-CHP; 3Helix Inc., Salt Lake City, UT) at 4°C overnight. Hematoxylin and eosin stainings were performed using routine procedures (Histoserve, Germantown, MD). To determine the wound index,[16] skin thickness was measured in four locations and the wound area was divided by the average skin thickness: wound index = (wound area)/average (skin thickness). The wound index, therefore, reflects the average width of the wound.[16]

Isolation of Adult Dermal Fibroblasts

Animals were euthanized and shaved, and dorsal skin was collected and cut into 1 × 1-mm pieces, which were plated in tissue culture dishes and fed by dropwise addition of Dulbecco's modified Eagle's medium supplemented with 20% fetal bovine serum, penicillin/streptomycin, and amphotericin B (all from Thermo Fisher, Grand Island, NY). Tissues were removed when dermal fibroblasts (DFs) started to migrate onto the plate, and fibroblasts were from then on cultured in Dulbecco's modified Eagle's medium supplemented with 10% fetal bovine serum at 37°C in a humidified atmosphere of 5% CO_2.

Isolation of Wound Fibroblasts

Mice were anesthetized as described above, and 8-mm polyvinyl alcohol sponges (PVA Unlimited, Warsaw, IL) were implanted in s.c. pockets at the shoulder/lower neck area and flanks. Mice were euthanized 7 days later, and sponges were collected under aseptic conditions. For culture

of wound fibroblasts (WFs), polyvinyl alcohol sponges were cut into pieces and cultured in Dulbecco's modified Eagle's medium supplemented with 20% fetal bovine serum, penicillin/streptomycin, and amphotericin B. Sponges were removed when fibroblasts started to migrate onto the plate, and the medium was switched to Dulbecco's modified Eagle's medium supplemented with 10% fetal bovine serum.

Collagen Gel Contraction Assay

Fibroblasts (1×10^5 cells/mL) were suspended in culture medium containing 0.75 mg/mL collagen I (Collagen I; high concentration; Corning, Glendale, AZ); 500 μL cell suspension was added into wells of a 12-well plate, and the collagen polymerized at 37°C. Once solid, the gel was overlaid with 200 μL culture medium. After 2 days, the stressed collagen gel was released from the well wall and allowed to contract for 1 more day. Images of the gels were taken, and the area of gels was measured in Fiji 3/ImageJ 2.1.0/1.53c (*https://imagej.net/software/fiji*, last accessed September 24, 2021).

In Situ Zymography

Dye-quenched (DQ) collagen I was dissolved in a concentration of 30 μg/mL in Dulbecco's phosphate-buffered saline (with Ca^{2+} and Mg^{2+}) containing 1% low gelling temperature agarose, rhodamine-phalloidin (1 U/mL), and DAPI (0.1 μg/mL) (all from Thermo Fisher). The mixture was cooled to 60°C and pipetted onto the prewarmed (45°C) microscopy slide, then the cell-bearing circular coverslip was flipped onto the agarose drop face down and the assembly was placed on ice. After the agarose had gelled, samples were incubated at 37°C in a humid chamber for 1 to 2 hours and fixed in 4% neutral-buffered formaldehyde (4°C; overnight) before imaging.

To inhibit matrix metalloprotease (MMP) activity, cells were pretreated with the MMP-inhibitor Galardin (10 μmol/L; also known as Ilomastatin or GM6001; Selleck, Houston, TX) or an equal volume of dimethyl sulfoxide for 30 minutes, and Galardin (10 μmol/L) or dimethyl sulfoxide was also added to the DQ collagen I/phalloidin/DAPI agarose mixture.

Immunofluorescence

Cells were fixed with 4% neutral-buffered paraformaldehyde (15 minutes; room temperature), and autofluorescence was blocked with 0.1 mol/L glycine (Sigma, St. Louis, MO) for 10 minutes at room temperature. Cells were permeabilized with 0.2% Triton X-100 (BioRad, Hercules, CA) for 15 minutes at room temperature, and unspecific protein binding was blocked with 0.5% casein (Sigma) in phosphate-buffered saline. Samples were then incubated with primary antibodies in 0.05% casein/phosphate-buffered saline overnight (4°C). Antigens were visualized by incubation with Alexa 488−conjugated secondary antibody in 0.05% bovine serum albumin/phosphate-buffered saline. Nuclei were labeled with DAPI (0.1 μg/mL). Specimens were mounted with ImmuMount (Thermo Fisher). Primary antibodies used were as follows: Smad2 (number 5339; Cell Signaling Technology, Danvers, MA) and Smad3 (number 28379; Abcam, Waltham, MA).

Microscopy

Specimens were imaged using a Keyence inverse microscope (Keyence, Itasca, IL), Aperio/Halo (Leica Biosystems, Deer Park, IL; and IndicaLabs, Albuquerque, NM), or a Leica SP8 confocal microscope (Leica Biosystems) and analyzed in HALOLink 3.3.14993.118 (IndicaLabs) or Fiji 3/ImageJ 2.1.0/1.53c (*https://imagej.net/software/fiji*, last accessed September 24, 2021). Collagen anisotropy was analyzed with the FibrilTool.[17]

Two-photon microscopy was performed using an inverted laser-scanning two-photon microscope (MPE-RS; Olympus, Center Valley, PA) equipped with a tunable laser (Insight DS+; Spectra Physics, Santa Clara, CA) and an Olympus USPLAPO 30× (numerical aperture, 1.05) silicone oil objective. Acquisition was performed using a galvo scanner. Excitation was performed at 900 nm, and the emitted light was collected by an appropriate set of mirrors and filters on three detectors (bandpass filters: blue = 410 to 460 nm; green = 495 to 540 nm; and red = 575 to 645 nm). Images were analyzed using Fiji 3/ImageJ 2.1.0/1.53c.

Gelatin Zymography

To assess MMP activity, Brij35 (Sigma) was added to cell-free culture supernatants to a concentration of 0.02% and samples were stored at −20°C before electrophoresis under nonreducing conditions using 8% or 10% polyacrylamide gels containing 0.1% gelatin (Fluka Chemie, Buchs, Switzerland). Gels were washed in 2.5% Triton X-100, followed by overnight incubation in 1% Triton X-100, 5 mmol/L $CaCl_2$, 1 μmol/L $ZnCl_2$, and 50 mmol/L Tris/HCl (pH 7.4); MMP activity was visualized by Coomassie Blue staining.

RNA Isolation and Real-Time Quantitative RT-PCR (RT-qPCR)

Fibroblasts were seeded at 500,000 cells/60-mm dish and allowed to grow for 3 days. RNA was isolated using the RNAEasy Plus Minikit (Qiagen, Germantown, MD) with a 15-minute DNAase digest (RNase-Free DNase Set; Qiagen), according to the manufacturer. For RT-qPCR, 0.5 to 2 μg RNA was transcribed using the High-Capacity cDNA Reverse Transcription Kit (Thermo Fisher), according to the manufacturer's instructions, and RT-qPCR was performed using the Power SYBR Green PCR Master Mix (Thermo Fisher) and specific primers (Table 1).

Table 1 Primers Used

Primer name	Primer sequence
Mouse_Ccn2_476_F	5′-AGAACTGTGTACGGAGCGTG-3′
Mouse_Ccn2_585_R	5′-GTGCACCATCTTTGGCAGTG-3′
Mouse_Ccn4_107_F	5′-CAGCACCACTAGAGGAAACGA-3′
Mouse_Ccn4_243_R	5′-CTGGGCACATATCTTACAGCATT -3′
Mouse_Col15a1_3053_F	5′-AAGGGTGCCAAAGGAGATCG-3′
Mouse_Col15a1_3211_R	5′-AGCGGTACCAACTGGTGTTT-3′
Mouse_Col18a1_4228_F	5′-TCTATAGCATCGTGCGCCGT-3′
Mouse_Col18a1_4460_R	5′-GTAACTCTCCATCAGCCTCCG-3′
Mouse_Lox_255_F	5′-TCTTCTGCTGCGTGACAACC-3′
Mouse_Lox_371_R	5′-GAGAAACCAGCTTGGAACCAG-3′
Mouse_Mmp2_105_F	5′-CAAGTTCCCCGGCGATGTC-3′
Mouse_Mmp2_275_R	5′-TTCTGGTCAAGGTCACCTGTC-3′
Mouse_Mmp3_1382_F	5′-GACTCAAGGGTGGATGCTGT-3′
Mouse_Mmp3_1451_R	5′-CCAACTGCGAAGATCCACTG-3′
Mouse_Mmp9_136_F	5′-GCAGAGGCATACTTGTACCG-3′
Mouse_Mmp9_364_R	5′-TGATGTTATGATGGTCCCACTTG -3′
Mouse_Mmp13_24_F	5′-CTTCTTCTTGTTGAGCTGGACTC -3′
Mouse_Mmp13_196_R	5′-CTGTGGAGGTCACTGTAGACT-3′
Mouse_P4ha1_1086_F	5′-AGCCACCATTTCAAACCCAGT-3′
Mouse_P4ha1_1156_R	5′-GCCAAGCACTTTTGCTAATTCTG -3′
Mouse_Plod2_225_F	5′-GAGAGGCGGTGATGGAATGAA-3′
Mouse_Plod2_337_R	5′-ACTCGGTAAACAAGATGACCAGA -3′
Mouse_Timp3_550_F	5′-CAACTCCGACATCGTGATCC-3′
Mouse_Timp3_679_R	5′-CACGTGGGGCATCTTACTGA-3′
Mouse_Tnc_4673_F	5′-TTCACAGTTTCCTGGACGGC-3′
Mouse_Tnc_4664_R	5′-TGTTTGGTGCCCTTGAGTGA-3′
Mouse_Serpine1 (Pai-1) _F	5′-CCCTGGCCGACTTC-3′
Mouse_Serpine1 (Pai-1) _R	5′-ACCTCGATCCTGAC-3′
Mouse_UBC_54_F	5′-CCACACAAAGCCCCTCAATC—3′
Mouse_UBC_123_R	5′-AAAGATCTGCATCGTCTCTCTC—3′
Mouse_Fn1	QuantiTect QT00136758 (Qiagen)

F, forward; R, reverse.

Data Analysis

Data were analyzed with GraphPad Prism 9.3.1 (GraphPad, San Diego, CA) using appropriate tests, as indicated. Briefly, the following were used: two samples, *t*-test; three or more samples, gaussian distribution: analysis of variance.

Results

Loss of Smurf2 Accelerates Early Phase of Wound Healing Process

To examine the effect of Smurf2 on wound healing, the full-thickness cutaneous incisional wound model was applied to the *SF2KO* and *WT* control mice and the wound healing process was followed thereafter. Three days after dermal incision, the wounds appeared to heal faster in *SF2KO* mice than in *WT* control mice, as evident by the narrower wounds on inspection of hematoxylin and eosin—stained skin sections (Figure 1A). By 14 days, wounds in SF2KO mice formed a narrow band, reminiscent of a tornado funnel (Figure 1A), and again were narrower than in *WT* animals. To statistically assess this observation, the wound index that reflects the width of the wound was calculated. *SF2KO* mice had a significantly lower wound index than their *WT* counterparts (Figure 1B). The difference in the wound index between *SF2KO* and *WT* mice gradually tapered toward the end of the 14-day experimental period as the healing process in the *WT* mice slowly caught up with that of *SF2KO* mice (Figure 1B).

Inflammation, the second phase of the wound healing response, is characterized by infiltration of neutrophils, macrophages, and lymphocytes, which are crucial for clearance of invading microbes and cellular debris, and subsequent formation of granulation tissues.[18] TGF-β/Smad3 signaling has been shown to promote migration of inflammatory cells into the wound.[7] On hematoxylin and eosin—stained sections, the area infiltrated with immune cells was wider in *SF2KO* mice than in *WT* controls 3 days after wounding (Figure 1A). This observation was corroborated by immunostaining of sections with the pan-immune cell marker CD45 (Figure 1A). Quantification of the infiltration of immune cells around the wound area as a surrogate measure of inflammation showed that inflammatory infiltration around the wound area was wider in *SF2KO* mice 3 days after wounding (Figure 1C). Immune infiltration around the wound was resolved at 14 days, but a trend toward a wider area around the wound being infiltrated in *SF2KO* wounds persisted (Figure 1C).

Smurf2 Regulates Stromal Strength and Collagen Morphology

Because *SF2KO* wounds healed fast, the stromal strength of wounds was examined next by measuring wound breaking strength with a universal testing machine at the end of 14-day experimental period. The results showed a trend of increased wound breaking strength for *SF2KO* mice compared with their *WT* counterparts, suggesting a more stable scar formation on loss of *Smurf2* (Figure 2A). Interestingly, the increased wound breaking strength was more striking in the female *SF2KO* mice, possibly due to an intrinsic higher breaking strength in *WT* male mice (Figure 2A). The trend of increased breaking strength associated with *Smurf2* loss was also present in normal skin and again was statistically significant in female mice (Figure 2A). These results indicate that the increase in wound breaking strength and narrower wounds, which are associated with loss of *Smurf2*, are likely caused by changes in underlying skin properties.

Early on during wound healing, granulation tissues are well demarcated, and the morphology of the deposited collagen is immature as it bundles to align in parallel. As the wound heals, collagen is organized in a basket-weave pattern,

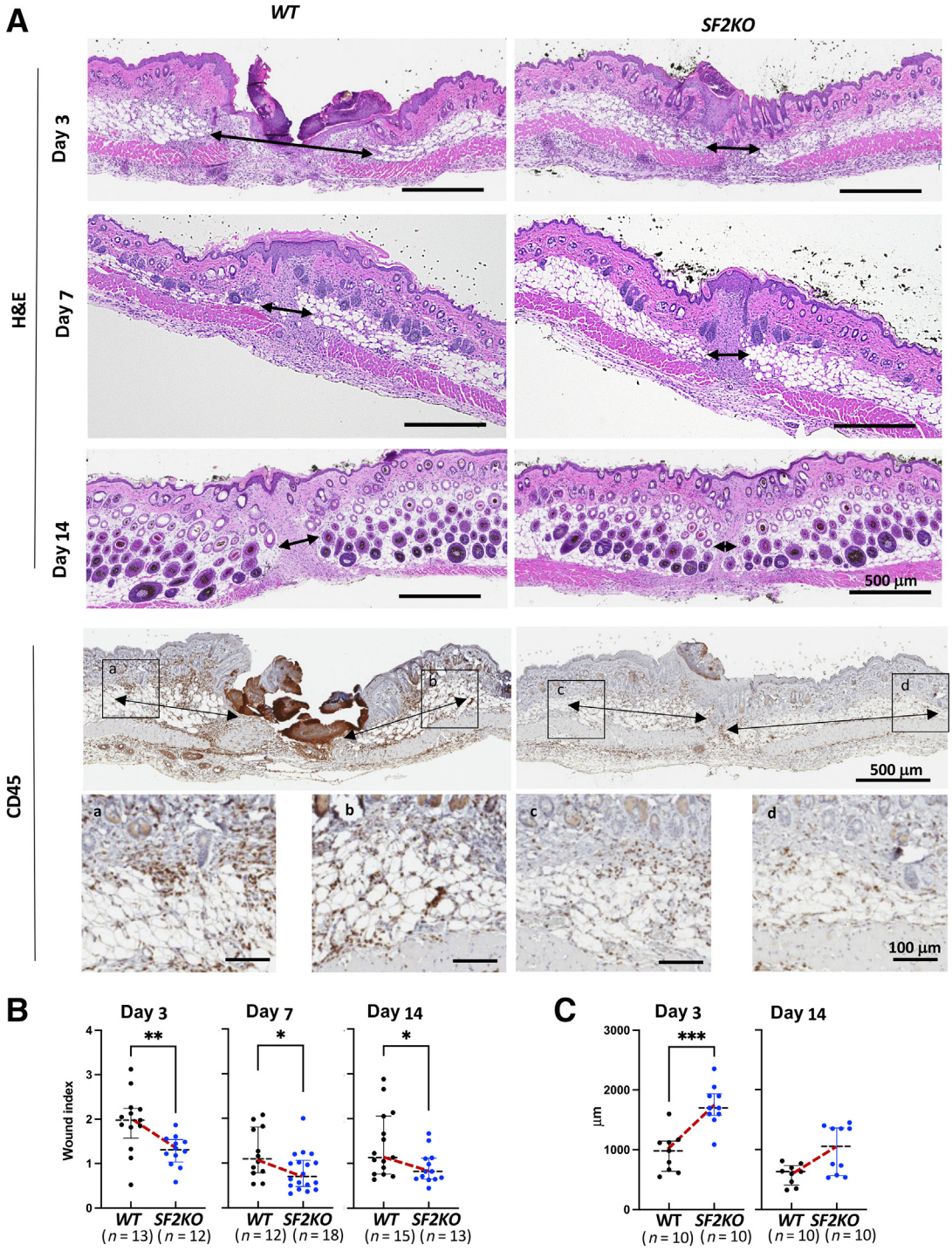

Figure 1 *Smurf2* loss leads to narrower wounds with increased inflammatory infiltration. **A:** Full-thickness dermal incisional wounding leads to narrower wounds in *SF2KO* mice compared with *WT* mice. **Top panels:** Hematoxylin and eosin (H&E) staining sections of wounds 3, 7, and 14 days after wounding are shown, and wound widths are indicated by **double-pointed arrows**. **Bottom panels (first row):** CD45 immunohistochemistry of wounds 3 and 14 days after wounding. Areas with inflammatory infiltration are indicated by **double-pointed arrows**. **Bottom panels (last row):** The marked areas are shown in higher magnification. **B:** Analysis of H&E images using the wound index (wound index = wound area/skin thickness). **C:** Inflammatory infiltration around wounds is wider in *SF2KO* animals than in *WT* animals. The data represent the average width (radius) of inflammatory infiltration around the wound. **B** and **C:** Medians are connected by **red dashed lines**. Data are given as median ± interquartile range (**B** and **C**). $^{*}P < 0.05$, $^{**}P < 0.01$, and $^{***}P < 0.001$. Scale bars: 500 μm [**A, top** and **bottom** (**first row**) **panels**]; 100 μm [**A**, **bottom panels** (**last row**)].

and its orientation and bundling are adapted to suit the local mechanical stresses on the skin.[19] Because *SF2KO* wounds tended to have higher breaking strength, the effect of *Smurf2* loss on collagen morphology in skin adjacent to wounds was examined next. *WT* skin showed the basket-weave morphology of mature collagen (Figure 2B). In contrast,

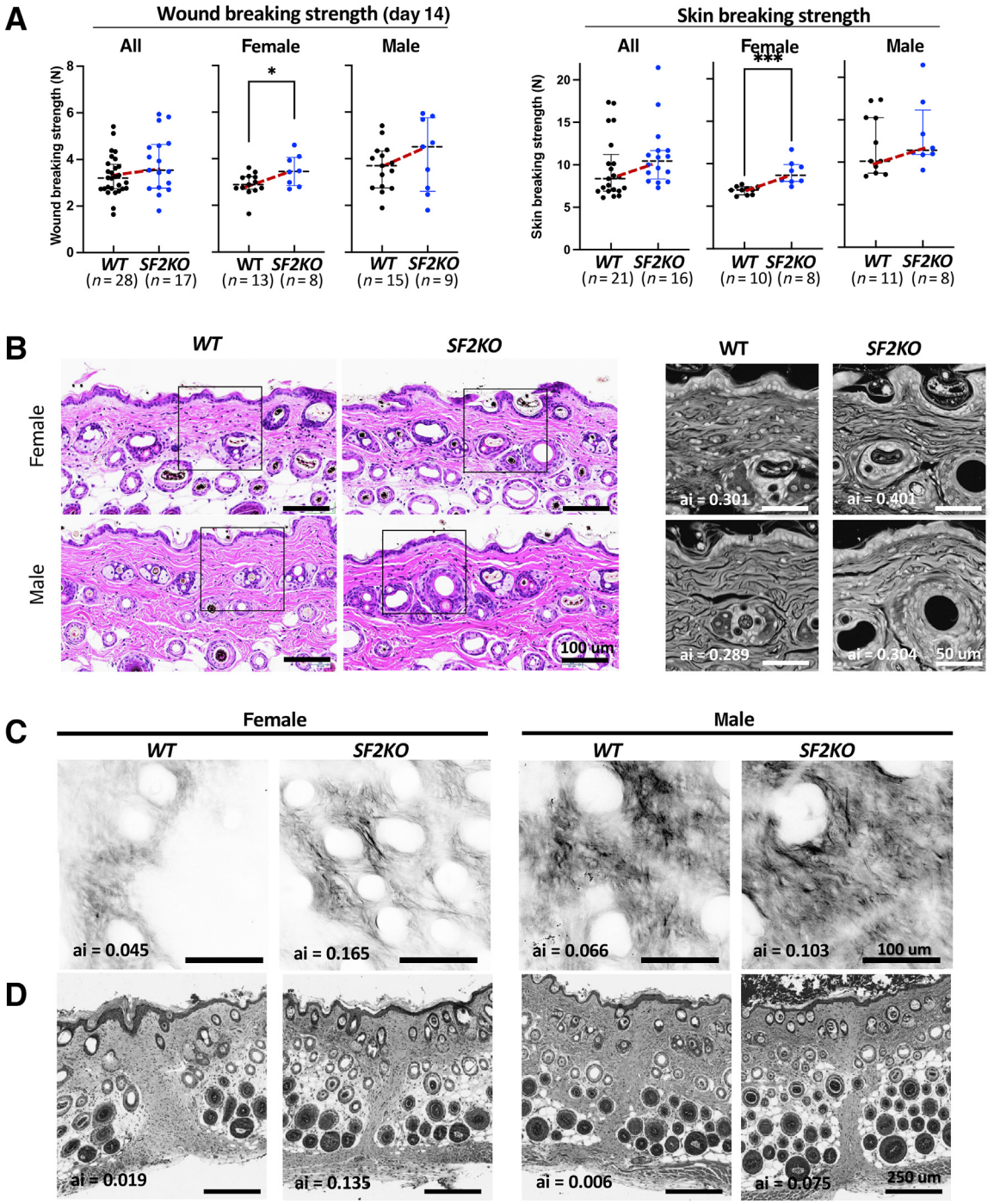

Figure 2 *Smurf2* loss leads to increased wound breaking strength and anisotropy of collagen bundles. **A:** Wound and skin breaking strength is higher in *SF2KO* mice than in *WT* mice. Wound and skin breaking strength were measured using a Universal testing machine. Medians are connected by **red dashed lines**. **B: Left panels:** Hematoxylin and eosin (H&E) staining of normal skin adjacent to the wound shows linearization of dermal collagen bundles. **Right panels:** The marked areas are shown at higher magnification. For easier visibility, the channels were split, and the blue channel was converted to grayscale and color inverted. FibrilTool was used to determine the anisotropy index (ai). **C:** Two-photon microscopy shows higher collagen linearization in ears of *SF2KO* animals. Images of mouse ears were taken at the level of the hair follicle, and the anisotropy index was obtained. **D:** *Smurf2* loss leads to higher anisotropy of collagen bundles in the subdermal wound tissue. To analyze anisotropy, channels of the H&E images shown in Figure 1A were split, and the blue channel was converted to grayscale and color inverted. Data shown as median ± interquartile range (**A**). $*P < 0.05$, $***P < 0.001$ (unpaired *t*-test). Scale bars: 100 μm (**B**, **left panels**, and **C**); 50 μm (**B**, **right panels**); 250 μm (**D**).

collagen bundles in *SF2KO* skin appeared coarser and more linear. Indeed, analysis of hematoxylin and eosin–stained sections with ImageJ/FibrilTool[17] revealed higher anisotropy of collagen bundles in *SF2KO* skin adjacent to the wound (Figure 2B), and two-photon microscopy of mice ears also showed higher anisotropy of collagen bundles in *SF2KO*

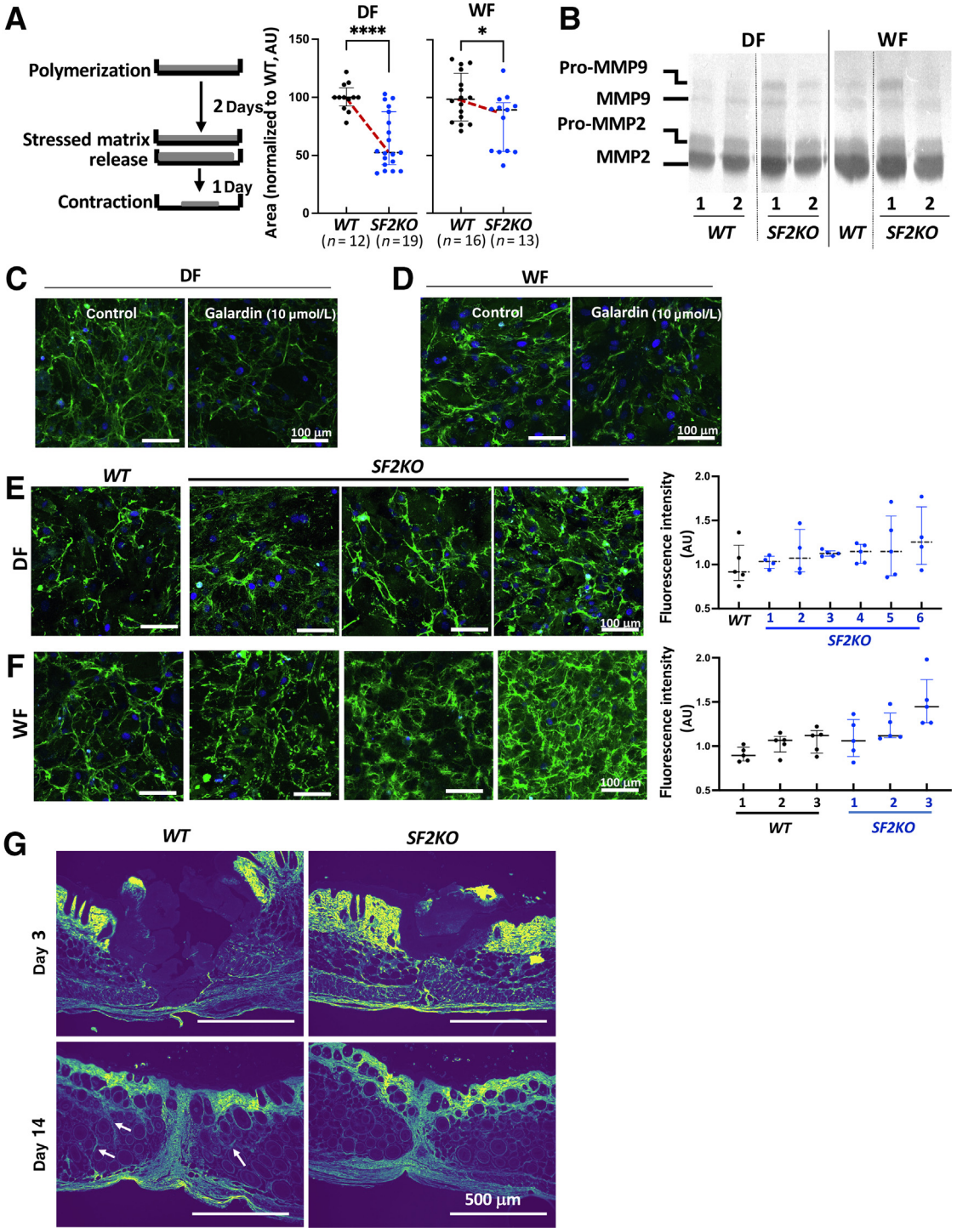

Figure 3 *Smurf2* loss changes fibroblast properties. **A:** *Smurf2* loss leads to increased contractility of fibroblasts, as shown in collagen gel contraction assay. Cells were seeded in collagen gels and allowed to form a stressed matrix, which was released after 2 days. The size (area) of the collagen gel was measured 1 day later. Medians are connected by **red dashed lines**. **B:** Gelatin zymography of culture supernatant shows increased levels of matrix metalloprotease (Mmp) 9/pro-Mmp9 in *SF2KO* dermal fibroblast (DF) and wound fibroblast (WF) cultures compared with the respective wild-type (WT) cells. **C** and **D:** The MMP-inhibitor Galardin (10 µmol/L) reduces gelatinolytic activity of DFs (**C**) and WFs (**D**) compared with the dimethyl sulfoxide (DMSO)—treated controls. Cells were pretreated with DMSO or Galardin before visualization of collagenolytic activity by *in situ* zymography DQ collagen I. **E** and **F:** *SF2KO* DFs (**E**) and WFs (**F**) have higher collagenolytic activity than in the respective WT cells, as shown by *in situ* zymography using DQ collagen. For quantification, 4 or 5 fields were imaged for each cell line. **G:** Visualization of denatured collagen using the collagen hybridization peptide R-CHP. Cross-sections of wounds show increased denatured collagen levels in areas surrounding the wound, most prominently the subdermal tissue, in *SF2KO* wounds 3 days after wounding. After 14 days, areas with increased denatured collagen levels remain in the subdermal tissue of *WT* wounds, whereas the *SF2KO* tissue shows little signal. **Arrows** indicate areas with increased R-CHP binding. Data shown as median ± interquartile range (**A**). $^{*}P < 0.05$, $^{****}P < 0.0001$ (unpaired *t*-test). Scale bars: 100 µm (**C**—**F**); 500 µm (**G**). AU, arbitrary unit.

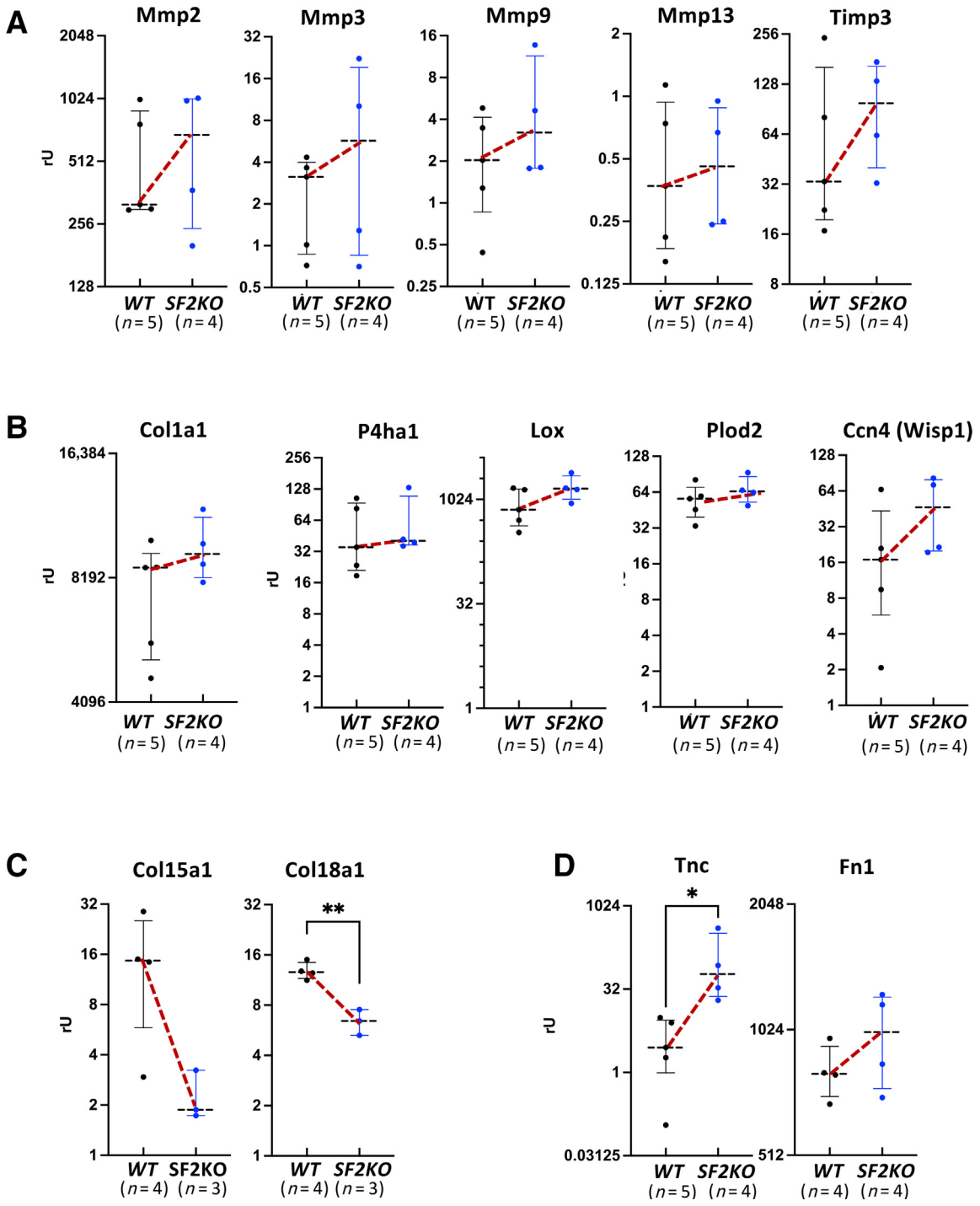

Figure 4 **A–D:** Loss of *Smurf2* changes expression of genes related to matrix turnover and cell contractility, as determined by RT-qPCR. *Ubiquitin C* (*Ubc*) expression was used for normalization. Medians are connected by **red dashed lines**. Data shown as median ± interquartile range (**A–D**). $^{*}P < 0.05$, $^{**}P < 0.01$ (unpaired *t*-test). Ccn4, cellular communication network factor 4; Col1a1, collagen type I alpha 1; Col15a1, collagen type 15 alpha 1; Col18a1, collagen type 18 alpha 1; Fn, fibronectin; Lox, lysyl oxidase; Mmp, matrix metalloprotease; P4ha1, prolyl 4-hydroxylase subunit alpha 1; Plod2, procollagen-lysine,2-oxoglutarate 5-dioxygenase 2; Timp, tissue inhibitor of metalloproteinases; Tnc, tenascin C; Wisp1, WNT1 inducible signaling pathway protein 1.

skin compared with *WT* skin (Figure 2C). Furthermore, collagen bundles in the prominent s.c. wound tissue 14 days after wounding had higher anisotropy in *SF2KO* mice (Figure 2D). Thus, loss of *Smurf2* led to changes in cutaneous collagen morphology, which could contribute to the increased wound breaking strength.

Smurf2 Regulates Fibroblast Contractility and Collagenolysis

Having shown that Smurf2 regulates wound healing and collagen morphology, the next step was to determine if these effects might be mediated by higher contractility of

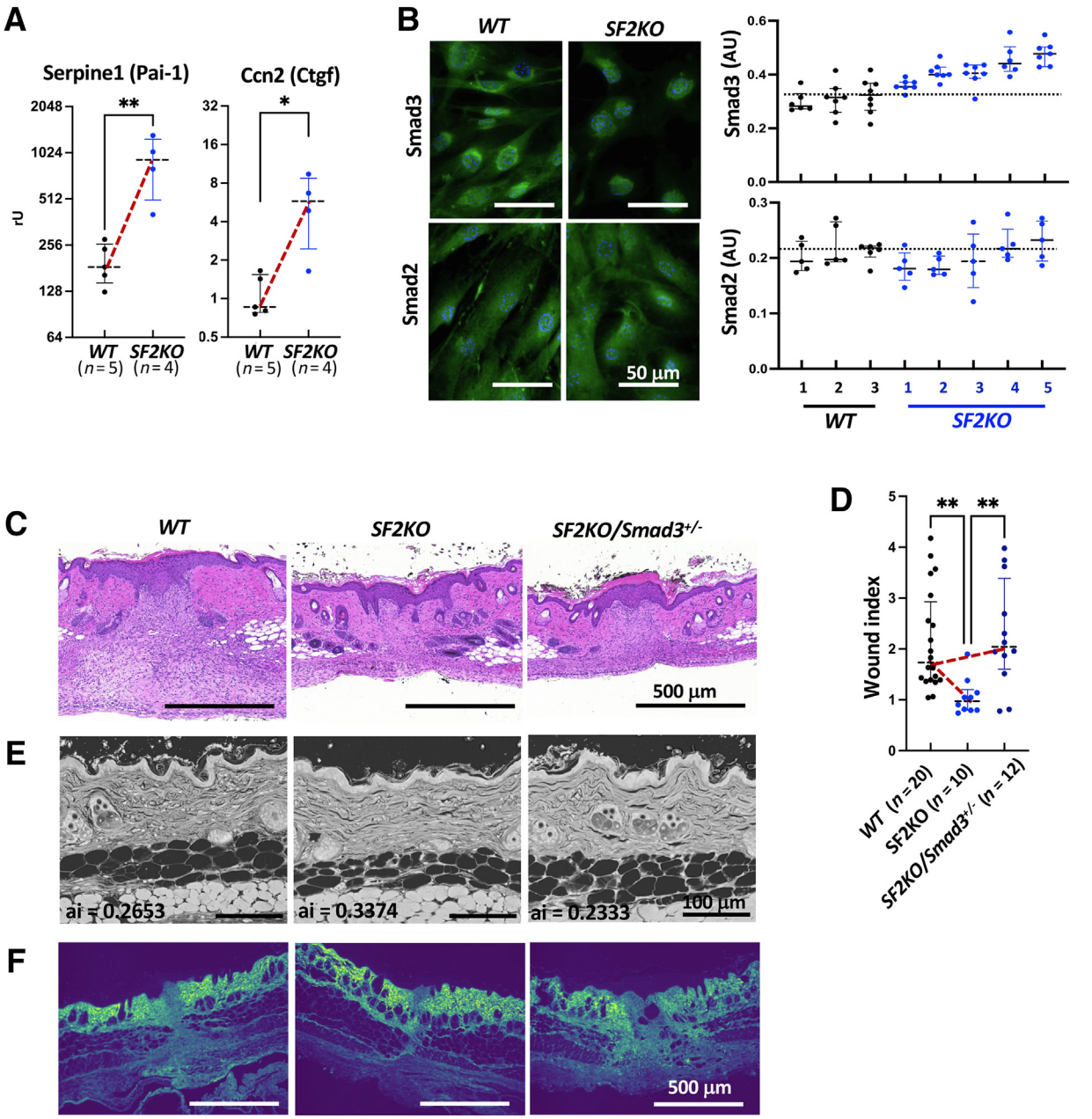

Figure 5 Haplo-insufficiency of *Smad3* in C57BL/6N animals attenuates effects of *Smurf2* loss on wound and collagen morphology. **A:** Loss of *Smurf2* increased expression of transforming growth factor-β/Smad3 target genes, *Serpine1* and *Ccn2*, as determined by RT-qPCR. *Ubc* expression was used for normalization. Unpaired *t*-test was used. Medians are connected by **red dashed lines**. **B:** *Smurf2* loss increases nuclear localization of Smad3 but not Smad2. **Left panels:** Localization of Smad2 and Smad3 was visualized by immunofluorescence. **Right panels:** DAPI label was used to identify the nuclear region, and the ratio of fluorescence intensity of nuclear Smad/total Smad fluorescence in the imaging field was calculated. **Black dotted lines** indicate the highest median Smad3 and Smad2 expression in *WT* samples. **C:** Hematoxylin and eosin staining of wounds 7 days after wounding shows that wounds of *SF2KO/Smad3*$^{+/-}$ mice are as wide as wounds of *WT* animals, whereas wounds in *SF2KO* animals are narrower. **D:** The wound index was used to quantify wound width. One-way analysis of variance was used. Medians are connected by **red dashed lines**. **E:** Haplo-insufficiency of *Smad3* attenuates the effect of *Smurf2* loss on collagen linearization in normal skin adjacent to the wound. Anisotropy was analyzed as in Figure 2, and anisotropy index (ai) was measured using FibrilTool. **F:** Visualization of denatured collagen using the collagen hybridization peptide R-CHP in wound sections at day 7 after wounding. Data shown as median ± interquartile range (**A** and **D**). $^{*}P < 0.05$, $^{**}P < 0.01$. Scale bars: 50 μm (**B**, **left panels**); 500 μm (**C** and **F**); 100 μm (**E**). AU, arbitrary unit; Ccn-2, cellular communication network factor-2; Ctgf, connective tissue growth factor; Pai-1, plasminogen activator inhibitor-1; rU, relative unit.

fibroblasts and if *Smurf2*-deficient fibroblasts more readily turn over collagen. Toward this end, normal DFs were isolated from unwounded normal skin and WFs were isolated from subcutaneously implanted polyvinyl alcohol sponges. To determine fibroblast contractility, collagen contraction assays (Figure 3A) were performed. Both DFs and WFs derived from *SF2KO* mice caused stronger contraction of the collagen I gels than their *WT* counterparts

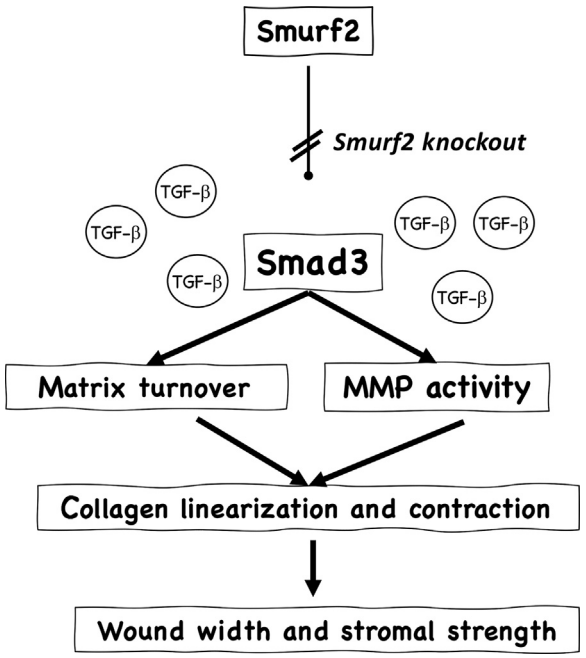

Figure 6 Role of Smurf2 in wound healing. Briefly, Smurf2 is known to inhibit Smad3 transcriptional activity. Removal of *Smurf2* leads to increased Smad3-mediated transforming growth factor (TGF)-β signaling. This results in changed expression of genes related to collagen processing and matrix metalloprotease (MMP) activity, which, in turn, causes linearization of cutaneous collagen and contraction. Consequently, the changes orchestrated by the removal of Smurf2 are beneficial to wound healing as expressed in narrower wounds with higher stromal strength.

(Figure 3A). Gelatin zymography was next used to detect gelatinase (Mmp-2 and Mmp-9) activity in cell-free culture supernatants. Mmp-9 levels were higher in *SF2KO* fibroblast cultures than in *WT* cultures (Figure 3B). *In situ* zymography with DQ collagen type I was performed to localize and detect collagenolytic activity of fibroblasts. In this assay, an increase of fluorescence directly reflects the level of collagenolytic activity of fibroblasts. As shown in Figure 3, C and D, both DFs and WFs degraded collagen type I. Collagen degradation was inhibited by the MMP-inhibitor Galardin, as indicated by the lower fluorescence on Galardin treatment. More importantly, *SF2KO* fibroblasts had higher collagenolytic activity than *WT* fibroblasts (Figure 3, E and F). Lastly, the collagen hybridization peptide R-CHP was used to detect denatured collagen in histologic specimens (Figure 3G). At day 3 after wounding, the subdermal tissue of *SF2KO* displayed higher levels of denatured collagen than that of *WT* controls (Figure 3G). After 14 days, however, little degraded collagen in the subdermal tissue around *SF2KO* wounds was observed, whereas the subdermal tissue around WT wounds still contained streaks of denatured collagen around *WT* scars (Figure 3G), indicating accelerated clearance of reactive tissue and wound healing in *SF2KO* animals. Thus, increased cell contractility and collagen degradation may account for the accelerated wound healing observed in *SF2KO* mice.

Smurf2 Regulates Gene Expression Related to Matrix Turnover and Contractility

Because *SF2KO* fibroblasts exhibited increased contractility and collagenolytic activity, such changes could also be reflected by changes in gene expression activities related to matrix turnover and cell contractility. Indeed, RT-qPCR showed that expression of *Mmp2*, *Mmp3*, *Mmp9*, and *Mmp13* was slightly increased in *SF2KO* WFs (Figure 4A). Notably, *Timp3*, a TGF-β/Smad3–regulated MMP inhibitor,[20,21] was also expressed higher in *SF2KO* WFs than in *WT* cells (Figure 4A). Thus, although collagenolytic activity was increased in *SF2KO* WFs, the activity of MMPs *in vivo* likely depends on the local balance of activation and inhibition of MMPs.

Expression of collagen type 1 (*Col1a1*) was also slightly increased in *SF2KO* WFs (Figure 4B), but collagen types 2 and 3 were mostly unchanged (data not shown). In addition, *Smurf2* loss increased expression of genes involved in collagen processing. Expression of *P4ha1*, *Lox*, and *Plod2*, which are enzymes involved in post-translational processing of the nascent collagen and in collagen cross-linking, was increased in *SF2KO* WFs (Figure 4B).[22–25] In addition, expression of *Ccn4* (*Wisp1*), an extracellular protein that recently has been shown to cause collagen linearization and scarless skin healing,[26] was increased and thus may account for the increased collagen linearization observed herein.

Other differentially expressed genes were *Col18a1* and *Col15a1* (Figure 4C). Both *Col18a1* and *Col15a1* were down-regulated in *SF2KO* WFs. Collagen 18 and collagen 15 are basement membrane collagens and yield degradation products, restin and endostatin, with anti-angiogenic properties.[27] *Col18a1* knockout in mice has been associated with slightly faster wound closure,[28] which might contribute to smaller wound index observed in *SF2KO* animals (Figure 1, A and B). Tenascin C (Tnc) is an adhesion-modulating extracellular protein that is expressed early during wound healing and can bind to the extracellular glue fibronectin[29] as well as integrins. As such, it can change cell spreading as well as signaling.[30] Lastly, expression of *Tnc* and fibronectin (*Fn1*) was increased in *SF2KO* WFs compared with that of *WT* WFs (Figure 4D).

Taken together, loss of *Smurf2* in WFs results in broad changes in matrix protein expression, which might lead to collagen linearization and increased cell contractility, as observed in *SF2KO* fibroblasts *in vitro* as well as *SF2KO* mice *in vivo*.

Haplo-Insufficiency of Smad3 Attenuates Changes Associated with Smurf2 Loss

Timp3, *Tnc*, and *Fn1* are known TGF-β–inducible genes[20,31,32] (Figure 4D). To further clarify whether TGF-β/Smad3 signaling is activated in *SF2KO* WFs, expression of classic TGF-β/Smad3–inducible genes, *Serpine1* (alias *Pai-1*) and *Ccn2* (alias *Ctgf*), was additionally analyzed. Both of

these well-characterized TGF-β/Smad3 transcriptional target genes were expressed higher in *SF2KO* WFs compared with *WT* WFs (Figure 5A). Furthermore, immunofluorescence showed higher nuclear localization of Smad3 but not of Smad2 in DFs and WFs (Figure 5B). These results indicate that loss of *Smurf2* leads to increased TGF-β/Smad3 signaling in fibroblasts.

To study whether the effect of Smurf2 on wound healing and collagen linearization is mediated by Smad3 signaling, one copy of *Smad3* gene was removed from *SF2KO* mice by breeding *SF2KO* mice with *Smad3*$^{+/-}$ mice. Because *Smad3* knockout *(Smad3*$^{-/-}$*)* mice were unhealthy and did not live long enough to allow for experimentation,[15] *SF2KO/Smad3*$^{+/-}$ mice were used in the full-thickness cutaneous incisional wound model. Seven days after the incision, the width and wound indexes of wounds in *SF2KO/Smad3*$^{+/-}$ and WT mice were comparable but larger or higher than those of the *SF2KO* wounds (Figure 5, C and D). Furthermore, reducing *Smad3* gene dosage attenuated the collagen linearization seen in unwounded normal skin of *SF2KO* mice (Figure 5E). Use of R-CHP revealed higher levels of denatured collagen in *WT* and *SF2KO/Smad3*$^{+/-}$ wounds compared with *SF2KO* wounds 7 days after wounding, indicating faster healing of *SF2KO* wounds (Figure 5F). These data indicate an important role of Smad3 in mediating the regulatory function of Smurf2 in wound healing.

Discussion

Wound healing is a highly conserved and tightly regulated response to trauma.[1] Poorly healed wounds are not only a cosmetic problem but rather can impair tissue functionality. Clinically, a narrow wound with greater breaking strength is highly desirable. TGF-β is a master regulator of wound healing and tissue fibrosis. Previous research has shown that the TGF-β–signaling protein Smad3 mediates inflammatory infiltration of wounds and granulation tissue formation.[7] The data presented herein show that loss of *Smurf2* via increased TGF-β/Smad3 signaling affects wound healing process by broad but subtle changes of expression of genes related to matrix production, turnover, and cell contractility, ultimately leading to narrower wounds and increased wound breaking strength (Figure 6).

Smurf2 is an E3 ubiquitin ligase that, among other substrates, ubiquitinates proteins of the TGF-β signaling family. Smurf2 inactivates Smad3 and thus gauges its activity; consequently, loss of Smurf2 can lead to increased Smad3 activity.[12] On a cellular level, TGF-β stimulation leads to myofibroblastoid differentiation of stromal cells and deposition of cellular matrix in tumors and wounds.[33] TGF-β/Smad3 signaling has been shown to increase granulation tissue formation and inflammatory infiltration in the previous study using an *Smad3* knockout mouse model,[34] which matches the observation herein that loss of *Smurf2* increases wound breaking strength. However, narrower wounds caused by *Smurf2* loss are counterintuitive to increased granulation tissue formation. It is possible that an earlier deposition of granulation tissue and altered qualities of the deposited collagen account for a different wound morphology.

Indeed, loss of Smurf2 leads to linearization of collagen (Figures 2 and 3). Mechanistically, TGF-β/Smad3 signaling is known to stimulate type I and type III collagen expression,[35] but has also been shown to up-regulate *Timp3*, *Mmp2*, and *Mmp9*, and to down-regulate the collagenase *Mmp1*.[20,35–39] Furthermore, TGF-β signaling regulates enzymes involved in collagen processing, like *Lox* and *Plod*,[40–43] and the matrix protein *Ccn4* (*Wisp1*), which has been recently described to change collagen linearization.[26] Herein, higher expression of *Lox* and *Plod2* as well as *Ccn4* was seen in *SF2KO* animals, making it likely that these enzymes are involved in collagen processing and specifically in the observed collagen linearization in the *SF2KO* mouse model. Interestingly, denatured collagen was initially higher, especially in the subdermal tissue adjacent to the wound in *SF2KO* animals, but later was cleared faster, pointing toward an accelerated wound healing in these animals (Figure 3G and Figure 5F).

Clinically, TGF-β/Smad3 signaling is increased in hypertrophic scars and keloids as well as in fibrotic tissues.[3,44–47] Smurf2 is up-regulated in hypertrophic scar fibroblasts derived from burn wounds.[48] In this model, increased Smurf2 leads to increased Smad7 degradation and subsequently to increased TGF-β signaling activity,[49] and down-regulation of Smurf2 by siRNA reduced collagen and smooth muscle actin expression.[48] In contrast, the results presented herein show that haploinsufficiency of *Smad3* at least partially reversed the wound healing phenotype induced by *Smurf2* loss, indicating that the effects of Smurf2 on wound healing are Smad3 dependent. These observations imply that Smurf2 might act on wound healing via two distinct and possibly competing mechanisms: it increases TGF-β signaling by Smad7 degradation, and it decreases TGF-β signaling by Smad3 inactivation. The data imply that a release of Smurf2 inhibition on Smad3 during early stages of wound healing leads to more favorable results, as measured by wound width and breaking strength, whereas later during chronic hypertrophic phase, Smurf2 might drive matrix deposition and contractures by releasing TGF-β signaling at the receptor level.

In summary, loss of *Smurf2* leads to Smad3-dependent changes in collagen morphology in unwounded normal skin, and subsequently increased wound breaking strength with decreased scarring after wounding. Clinically, manipulating Smurf2 E3 ligase activity might therefore be an attractive approach to optimize healing of wounds and scar formation. Analyzing the exact biochemical mechanism by which Smurf2 affects changes in matrix expression and scarring will likely reveal several co-operating signaling pathways and will be the subject of future work.

Author Contributions

C.H.S. conceived and designed research, performed the experiments, analyzed the data, and wrote the article; N.M. and B.S. performed the experiments; Y.T. designed research and maintained animals for the experiments; M.K. and J.P.F. performed the experiments and analyzed the data; R.W. provided critical equipment and resources; and Y.E.Z. conceived research, provided resources, and wrote the article.

Acknowledgments

We thank Dr. Baktiar Karim for pathology service; Cing Dim for animal husbandry; Ramiro Iglesias-Bartolome and Paul Randazzo for discussions; Yeap Ng for maintaining the buprenorphine stock and assistance with animal experiments; and Robert Choe for help with measuring skin breaking strength.

References

1. Schultz GS, Chin GA, Moldawer L, Diegelmann RF: Principles of wound healing. Edited by Fitridge R, Thompson M. In Mechanisms of Vascular Disease: A Reference Book for Vascular Specialists. Adelaide, Australia: University of Adelaide Press, 2011. pp. 423−451
2. Kiritsi D, Nyström A: The role of TGF[beta] in wound healing pathologies. Mech Ageing Dev 2018, 172:51−58
3. Finnson KW, McLean S, Di Guglielmo GM, Philip A: Dynamics of transforming growth factor beta signaling in wound healing and scarring. Adv Wound Care (New Rochelle) 2013, 2:195−214
4. Rognoni E, Watt FM: Skin cell heterogeneity in development, wound healing, and cancer. Trends Cell Biol 2018, 28:709−722
5. Heldin C-H, Moustakas A: Signaling receptors for TGF-[beta] family members. Cold Spring Harb Perspect Biol 2016, 8:a022053
6. Hata A, Chen Y-G: TGF-[beta] signaling from receptors to Smads. Cold Spring Harb Perspect Biol 2016, 8:a022061
7. Ashcroft GS, Yang X, Glick AB, Weinstein M, Letterio JL, Mizel DE, Anzano M, Greenwell-Wild T, Wahl SM, Deng C, Roberts AB: Mice lacking Smad3 show accelerated wound healing and an impaired local inflammatory response. Nat Cell Biol 1999, 1: 260−266
8. Zhang Y, Chang C, Gehling DJ, Hemmati-Brivanlou A, Derynck R: Regulation of Smad degradation and activity by Smurf2, an E3 ubiquitin ligase. Proc Natl Acad Sci U S A 2001, 98:974−979
9. Andrews PS, Schneider S, Yang E, Michaels M, Chen H, Tang J, Emkey R: Identification of substrates of SMURF1 ubiquitin ligase activity utilizing protein microarrays. Assay Drug Dev Technol 2010, 8:471−487
10. David D, Nair SA, Pillai MR: Smurf E3 ubiquitin ligases at the cross roads of oncogenesis and tumor suppression. Biochim Biophys Acta 2013, 1835:119−128
11. Lin X, Liang M, Feng XH: Smurf2 is a ubiquitin E3 ligase mediating proteasome-dependent degradation of Smad2 in transforming growth factor-beta signaling. J Biol Chem 2000, 275:36818−36822
12. Tang L-Y, Yamashita M, Coussens NP, Tang Y, Wang X, Li C, Deng C-X, Cheng SY, Zhang YE: Ablation of Smurf2 reveals an inhibition in TGF-[beta] signalling through multiple mono-ubiquitination of Smad3. EMBO J 2011, 30:4777−4789
13. Kavsak P, Rasmussen RK, Causing CG, Bonni S, Zhu H, Thomsen GH, Wrana JL: Smad7 binds to Smurf2 to form an E3 ubiquitin ligase that targets the TGF beta receptor for degradation. Mol Cell 2000, 6:1365−1375
14. Blank M, Tang Y, Yamashita M, Burkett SS, Cheng SY, Zhang YE: A tumor suppressor function of Smurf2 associated with controlling chromatin landscape and genome stability through RNF20. Nat Med 2012, 18:227−234
15. Yang X, Letterio JJ, Lechleider RJ, Chen L, Hayman R, Gu H, Roberts AB, Deng C: Targeted disruption of SMAD3 results in impaired mucosal immunity and diminished T cell responsiveness to TGF-beta. EMBO J 1999, 18:1280−1291
16. Zheng Z, Nguyen C, Zhang X, Khorasani H, Wang JZ, Zara JN, Chu F, Yin W, Pang S, Le A, Ting K, Soo C: Delayed wound closure in fibromodulin-deficient mice is associated with increased TGF-[beta]3 signaling. J Invest Dermatol 2011, 131:769−778
17. Boudaoud A, Burian A, Borowska-Wykręt D, Uyttewaal M, Wrzalik R, Kwiatkowska D, Hamant O: FibrilTool, an ImageJ plug-in to quantify fibrillar structures in raw microscopy images. Nat Protoc 2014, 9:457−463
18. Koh TJ, DiPietro LA: Inflammation and wound healing: the role of the macrophage. Expert Rev Mol Med 2011, 13:e23
19. van Zuijlen PPM, Ruurda JJB, van Veen HA, van Marle J, van Trier AJM, Groenevelt F, Kreis RW, Middelkoop E: Collagen morphology in human skin and scar tissue: no adaptations in response to mechanical loading at joints. Burns 2003, 29:423−431
20. Leivonen S-K, Lazaridis K, Decock J, Chantry A, Edwards DR, Kähäri V-M: TGF-[beta]-elicited induction of tissue inhibitor of metalloproteinases (TIMP)-3 expression in fibroblasts involves complex interplay between Smad3, p38α, and ERK1/2. PLoS One 2013, 8:e57474
21. Fan D, Kassiri Z: Biology of tissue inhibitor of metalloproteinase 3 (TIMP3), and its therapeutic implications in cardiovascular pathology. Front Physiol 2020, 11:661
22. Kurozumi A, Kato M, Goto Y, Matsushita R, Nishikawa R, Okato A, Fukumoto I, Ichikawa T, Seki N: Regulation of the collagen cross-linking enzymes LOXL2 and PLOD2 by tumor-suppressive microRNA-26a/b in renal cell carcinoma. Int J Oncol 2016, 48:1837−1846
23. Berthet E, Chen C, Butcher K, Schneider RA, Alliston T, Amirtharajah M: Smad3 binds Scleraxis and Mohawk and regulates tendon matrix organization. J Orthop Res 2013, 31:1475−1483
24. Rosell-García T, Palomo-Álvarez O, Rodríguez-Pascual F: A hierarchical network of hypoxia-inducible factor and SMAD proteins governs procollagen lysyl hydroxylase 2 induction by hypoxia and transforming growth factor [beta]1. J Biol Chem 2019, 294: 14308−14318
25. Onursal C, Dick E, Angelidis I, Schiller HB, Staab-Weijnitz CA: Collagen biosynthesis, processing, and maturation in lung ageing. Front Med (Lausanne) 2021, 8:593874
26. Jia H, Janjanam J, Wu SC, Wang R, Pano G, Celestine M, Martinot O, Breeze-Jones H, Clayton G, Garcin C, Shirinifard A, Zaske AM, Finkelstein D, Labelle M: The tumor cell-secreted matricellular protein WISP1 drives pro-metastatic collagen linearization. EMBO J 2019, 38:e101302
27. Karsdal MA, Nielsen SH, Leeming DJ, Langholm LL, Nielsen MJ, Manon-Jensen T, Siebuhr A, Gudmann NS, Rønnow S, Sand JM, Daniels SJ, Mortensen JH, Schuppan D: The good and the bad collagens of fibrosis - their role in signaling and organ function. Adv Drug Deliv Rev 2017, 121:43−56
28. Seppinen L, Sormunen R, Soini Y, Elamaa H, Heljasvaara R, Pihlajaniemi T: Lack of collagen XVIII accelerates cutaneous wound healing, while overexpression of its endostatin domain leads to delayed healing. Matrix Biol 2008, 27:535−546
29. Zollinger AJ, Smith ML: Fibronectin, the extracellular glue. Matrix Biol 2017, 60−61:27−37
30. Midwood KS, Chiquet M, Tucker RP, Orend G: Tenascin-C at a glance. J Cell Sci 2016, 129:4321−4327

31. Katoh D, Kozuka Y, Noro A, Ogawa T, Imanaka-Yoshida K, Yoshida T: Tenascin-C induces phenotypic changes in fibroblasts to myofibroblasts with high contractility through the integrin [alpha]v [beta]1/TGF-[beta]/SMAD signaling axis in human breast cancer. Am J Pathol 2020, 190:2123−2135
32. Ignotz RA, Massagué J: Transforming growth factor-beta stimulates the expression of fibronectin and collagen and their incorporation into the extracellular matrix. J Biol Chem 1986, 261: 4337−4345
33. Stuelten CH, Zhang YE: Transforming growth factor-[beta]: an agent of change in the tumor microenvironment. Front Cell Dev Biol 2021, 9:764727
34. Ashcroft GS, Horan MA, Ferguson MW: Aging is associated with reduced deposition of specific extracellular matrix components, an upregulation of angiogenesis, and an altered inflammatory response in a murine incisional wound healing model. J Invest Dermatol 1997, 108:430−437
35. Ghosh AK, Yuan W, Mori Y, Varga J: Smad-dependent stimulation of type I collagen gene expression in human skin fibroblasts by TGF-beta involves functional cooperation with p300/CBP transcriptional coactivators. Oncogene 2000, 19:3546−3555
36. Lu P, Wang S, Cai W, Sheng J: Role of TGF-[beta]1/Smad3 signaling pathway in secretion of type I and III collagen by vascular smooth muscle cells of rats undergoing balloon injury. J Biomed Biotechnol 2012, 2012:965953
37. Qureshi HY, Ricci G, Zafarullah M: Smad signaling pathway is a pivotal component of tissue inhibitor of metalloproteinases-3 regulation by transforming growth factor beta in human chondrocytes. Biochim Biophys Acta 2008, 1783:1605−1612
38. Yuan W, Varga J: Transforming growth factor-beta repression of matrix metalloproteinase-1 in dermal fibroblasts involves Smad3. J Biol Chem 2001, 276:38502−38510
39. Stuelten CH, DaCosta Byfield S, Arany PR, Karpova TS, Stetler-Stevenson WG, Roberts AB: Breast cancer cells induce stromal fibroblasts to express MMP-9 via secretion of TNF-alpha and TGF-beta. J Cell Sci 2005, 118:2143−2153
40. Gjaltema RAF, de Rond S, Rots MG, Bank RA: Procollagen lysyl hydroxylase 2 expression is regulated by an alternative downstream transforming growth factor [beta]-1 activation mechanism. J Biol Chem 2015, 290:28465−28476
41. Qi Y, Xu R: Roles of plods in collagen synthesis and cancer progression. Front Cell Dev Biol 2018, 6:66
42. Fang Y, Chang H-M, Cheng J-C, Klausen C, Leung PCK, Yang X: Transforming growth factor-[beta]1 increases lysyl oxidase expression by downregulating MIR29A in human granulosa lutein cells. Reproduction 2016, 152:205−213
43. Huang M, Liu Z, Baugh L, DeFuria J, Maione A, Smith A, Kashpur O, Black LD Iii, Georgakoudi I, Whitfield ML, Garlick J: Lysyl oxidase enzymes mediate TGF-[beta]1-induced fibrotic phenotypes in human skin-like tissues. Lab Invest 2019, 99:514−527
44. Zhang T, Wang X-F, Wang Z-C, Lou D, Fang Q-Q, Hu Y-Y, Zhao W-Y, Zhang L-Y, Wu L-H, Tan W-Q: Current potential therapeutic strategies targeting the TGF-[beta]/Smad signaling pathway to attenuate keloid and hypertrophic scar formation. Biomed Pharmacother 2020, 129:110287
45. Tan R, He W, Lin X, Kiss LP, Liu Y: Smad ubiquitination regulatory factor-2 in the fibrotic kidney: regulation, target specificity, and functional implication. Am J Physiol Renal Physiol 2008, 294: F1076−F1083
46. Cai Y, Huang G, Ma L, Dong L, Chen S, Shen X, Zhang S, Xue R, Sun D, Zhang S: Smurf2, an E3 ubiquitin ligase, interacts with PDE4B and attenuates liver fibrosis through miR-132 mediated CTGF inhibition. Biochim Biophys Acta Mol Cell Res 2018, 1865:297−308
47. Zhang Y, Qian H, Wu B, You S, Wu S, Lu S, Wang P, Cao L, Zhang N, Sun Y: E3 ubiquitin ligase NEDD4 family-regulatory network in cardiovascular disease. Int J Biol Sci 2020, 16:2727−2740
48. Zhang Z, Finnerty CC, He J, Herndon DN: Smad ubiquitination regulatory factor 2 expression is enhanced in hypertrophic scar fibroblasts from burned children. Burns 2012, 38:236−246
49. Zhang Z, Liu C, Chen B, Tang W, Liu Z, Cao W, Li X: Smad7 downregulation via ubiquitin degradation mediated by Smurf2 in fibroblasts of hypertrophic scars in burned patients. Burns 2021, 47:1333−1341